Atmos. Chem. Phys., 23, 1449–1464, 2023
https://doi.org/10.5194/acp-23-1449-2023

Atmospheric Chemistry and Physics
Open Access
EGU

Magnetic fraction of the atmospheric dust in Kraków – physicochemical characteristics and possible environmental impact

Jan M. Michalik[1], Wanda Wilczyńska-Michalik[2], Łukasz Gondek[1], Waldemar Tokarz[1], Jan Żukrowski[3], Marta Gajewska[3], and Marek Michalik[4]

[1]Department of Solid State Physics, y, Faculty of Physics and Applied Computer Science, AGH University of Science and Technology, A. Mickiewicza Av. 30, 30-059 Krakow, Poland
[2]Institute of Geography, Pedagogical University, ul. Podchorążych 2, 30-084 Kraków, Poland
[3]Academic Centre for Materials and Nanotechnology, AGH University of Science and Technology, A. Mickiewicza Av. 30, 30-059 Kraków, Poland
[4]Institute of Geological Sciences, Jagiellonian University, ul. Gronostajowa 3a, 30-387 Kraków, Poland

Correspondence: Jan M. Michalik (jmichali@agh.edu.pl)

Received: 8 June 2022 – Discussion started: 4 July 2022
Revised: 2 December 2022 – Accepted: 8 December 2022 – Published: 26 January 2023

Abstract. It is well established that airborne, magnetic nano- and microparticles accumulate in human organs (e.g. brain) thereby increasing the risk of various diseases (e.g. cancer, neurodegenerative diseases). Therefore, precise characterization of the material, including its origins, is a key factor in preventing further, uncontrolled emission and circulation. The magnetic fraction of atmospheric dust was collected in Kraków using a static sampler and analysed using several methods (scanning electron microscopy with energy-dispersive spectrometry, transmission electron microscopy with energy-dispersive spectrometry, X-ray diffraction, Mössbauer spectroscopy, and vibrating sample magnetometry (VSM) measurements). The magnetic fraction contains magnetite, hematite and α-Fe, as well as quartz, feldspar and pyroxene often attached to the magnetic particles. The magnetic particles vary in size, from over 20 µm to nanoparticles below 100 nm, as well as in morphology (irregular or spherical). Their chemical composition is dominated by Fe, often with Mn, Zn, Cr, Cu, Si, Al, S, Ca and other elements. Mössbauer spectroscopy corroborates the composition of the material, giving further indications of particles smaller than 100 nm present in the atmospheric dust. VSM measurements confirm that the strength of the magnetic signal can be treated as a measure of the anthropogenic impact on the suspended particulate matter, once again highlighting the presence of nanoparticles.

1 Introduction

The magnetic fraction of atmospheric dust can be considered as a main carrier of metals, especially Fe and transition metals. Usually, the magnetic properties of the total particulate matter samples (e.g. PM_{10}, $PM_{2.5}$, PM_1) are analysed (Górka-Kostrubiec et al., 2020; Morris et al., 1995; Muxworthy et al., 2003; Petrovský et al., 2013; Revuelta et al., 2014; Sagnotti et al., 2006; Spassov et al., 2004; Wang et al., 2017). Baatar et al. (2017) studied the magnetic properties of atmospheric dust removed from the atmosphere during rainfall. The magnetic characteristics of the atmospheric particulate matter is sometimes studied using dust fall samples (e.g. Liu et al., 2019; Magiera et al., 2010). The magnetic properties of particles deposited on biological surfaces can be useful in terms of the biomagnetic monitoring of atmospheric pollution (Hofman et al., 2017; Maher, 2009; Mejía-Echeverry et al., 2018). Rutkowski et al. (2020) studied the magnetic parameters of dust deposited on spider webs.

The magnetic fraction of atmospheric particulate matter is rarely collected separately using specially constructed samplers (Cheng et al., 2018, 2014; Wirth and Prodi, 1972). Mag-

netic fraction collected separately, even containing an admixture of non-magnetic particles, enables a more precise characterization of magnetic particles compared with total particulate matter sample (e.g. PM_{10}).

Zhang et al. (2020), determined (after extraction from $PM_{2.5}$ samples) an annual mean concentration of magnetite nanoparticles (with a relatively broad distribution from 80 to 230 nm) in the urban atmosphere in Beijing to be $75.5 \pm 33.2\,ng\,m^{-3}$ and the daily intake of magnetite was estimated to be 16.6 ± 7.3, 29.5 ± 13, and $36.4 \pm 16\,ng\,kg^{-1}$ of body weight (bw) per day for adults, children, and toddlers respectively. For outdoor professions the intake value can reach $42\,ng\,kg^{-1}\,bw\,d^{-1}$.

Metal-containing particles are hazardous for human health (e.g. Sorensen, 2005; Zhang et al., 2020). The toxicity of metallic particles is related, among others, to the oxidative stress. The effect is significant for transition metal-containing particles because of Haber–Weiss and Fenton-type reactions (Biswas and Wu, 2005; Manke et al., 2013). Morris et al. (1995) proved the correlation between magnetic susceptibility and the mutagenicity of organic extracts from filters containing PM_{10} particulate matter. Maher et al. (2016) proved that magnetite nanoparticles present in the human brain are of airborne origin. Magnetite pollution nanoparticles may constitute a risk factor for Alzheimer's and Parkinson's diseases (Calderón-Garcidueñas et al., 2019; Gonet and Maher, 2019; Maher, 2019). Calderón-Garcidueñas et al. (2019) identified combustion- and friction-derived Fe-rich, strongly magnetic nanoparticles in the hearts of residents of polluted cities. Lu et al. (2020) identified exogenous nanoparticles containing Fe and other transition metals and metalloids in human serum and pleural effusion.

Metals (e.g. Fe, Ti, Mn) in aerosol particles are active in the catalytic oxidation of SO_2 in the atmosphere and in the formation of sulphate aerosol (Alexander et al., 2009; Dupart et al., 2012). Dust acts as a carrier of nutrients (e.g. Fe, P) transported to aquatic environments (Baker et al., 2006; Buck et al., 2010) and consequently it can modify processes in the biosphere by providing various elements (e.g. Zn, Cu, Mn) (e.g. Mackey et al., 2015; Mahowald et al., 2018; Paytan et al., 2009). Fe-rich particles are commonly dark coloured and participate in the heating effect of the atmosphere (Moteki et al., 2017). It was evaluated that aggregated magnetite nanoparticles from anthropogenic sources contribute to 4 %–7 % of the shortwave absorption of black carbon (Ito et al., 2018).

The aim of the present study was to characterize the magnetic fraction of aerosols in Kraków. Because collection of the analytical material is very important in such a study, a simple passive sampler was prepared and used for that purpose.

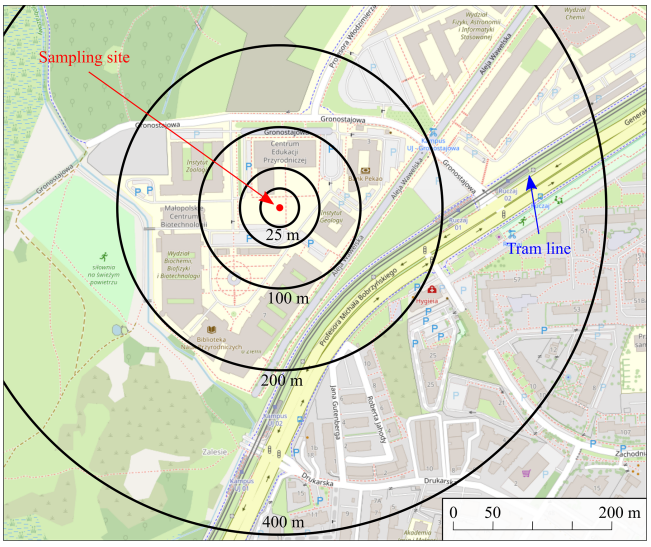

Figure 1. Sampling site: 50.026916979306854° N, 19.902035577195356° E (on the basis of © OpenStreetMap contributors 2012. Distributed under the Open Data Commons Open Database License (ODbL) v1.0).

2 Methods

2.1 Magnetic fraction collection and experimental protocol

To collect the magnetic fraction of atmospheric dust, a static (passive) sampler composed of a matrix of solid magnets arranged to increase gradients and magnetic field strength was used. It was covered with a 25 µm thick PVC film in order to ease the separation of the collected sample from the sampler itself. Two double collecting surfaces were situated vertically ca. 1.5–1.7 m above the surface of ground covered by grass. The sampling site was situated at the III Campus of Jagiellonian University (Gronostajowa Street, Kraków, Poland) – see Fig. 1 (please refer to the file "Supplement A" in the Supplement for more detailed information on the sampler and the sampling site). We collected the sample for 9 months (which covers several seasons). However, the particles we aim to trace are formed either in high-temperature industrial processes or may be related to other activities with no seasonal variations (e.g. transport). Consequently winter/summer differences are not as important as in the case of the investigation of coal or other fuel-burning products for household heating (e.g. soot).

After the PVC foil was removed from the magnets' matrix it was submerged in isopropyl alcohol and placed in an ultrasonic bath in order to detach all the collected material. Then a small fraction of the material was separated for the preparation of specimens for scanning electron microscopy. The rest of the sample was used for consecutive measurements – magnetometry, Mössbauer spectroscopy and X-ray diffrac-

tion (on a collected sample after grounding and on a fraction magnetically separated after grinding).

2.2 Scanning and transmission electron microscopy with energy-dispersive spectrometry

A field emission scanning electron microscope ([FE-SEM], HITACHI S-4700) equipped with an X-ray energy-dispersive spectrometer ([EDS], NORAN NSS) was used to study the morphology of the components of the magnetic fraction and their chemical composition. Samples mounted on adhesive carbon discs were carbon coated. Both secondary electron (SE) and backscattered electron (BSE) modes were used for imaging. An accelerating voltage of 20 kV, 10 µA current and 100 s counting time were applied for the chemical analyses. The standardless method was applied for the quantification of the chemical elements. Transmission electron microscopy (TEM) investigations were carried out on a Tecnai TF20 X-TWIN FEG microscope (Thermo Fisher Scientific, working at an accelerating voltage of 200 kV), equipped with an energy-dispersive X-ray detector (EDAX). Samples for the TEM observations were prepared by the drop casting of isopropyl alcohol/atmospheric dust dispersion on carbon-coated copper TEM grids. Bright field (BF), scanning transmission electron microscopy (STEM) and high-resolution transmission electron microscopy (HRTEM) observations were performed, as well as chemical (EDS) and electron diffraction (selected area electron diffraction [SAED]) analyses.

2.3 Mössbauer spectroscopy and magnetization measurements

^{57}Fe Mössbauer measurements were carried out in the transmission mode utilizing a constant acceleration spectrometer with ^{57}Co in a rhodium matrix as a source. Low-temperature measurements were carried out in a cold finger type cryostat filled with liquid nitrogen. Due to a very low mass of the sample and in order to assure optimal absorbent thickness keeping measurement time reasonable (i.e. both the Fe concentration and the dimensions), it was mixed with a filler (sucrose was chosen due to ease in its removal before the subsequent measurements). The obtained spectra were fitted using the Gauss–Newton iterative method of minimizing the chi^2, with a Lorentzian shape of the spectral lines. Magnetic isothermal loops M(H) at room temperature as well as at liquid nitrogen temperature were measured in a range up to 10 kOe using the Lake Shore Vibrating Sample Magnetometer model 7300 (VSM). The temperature stability was monitored during the measurements. Zero-field-cooled (ZFC) and field-cooled (FC) magnetic curves were also measured.

2.4 X-ray diffraction analysis

X-ray diffraction (XRD) measurements were made by means of a Malvern Panalytical Empyrean powder diffractometer using Cu K_α radiation. The powdered samples were placed on single-crystalline silicon zero-background holders. The measurements were performed primarily on the samples without any treatment. Unfortunately, the contribution originating from SiO_2 surpasses reflections from other phases. Therefore, the samples were grounded and suspended in distilled water in the presence of a magnetic field in order to separate the magnetic fractions, which were the main interest. This process significantly improved the chances of identifying other phases. The collected diffraction patterns were analysed according to the Rietveld method using the FullProf Suite Package (Rodríguez-Carvajal, 1993). The FullProf Suite was used solely for Rietveld refinement, which resulted in quantification of the observed crystalline phases. The phase identification was a multistep process that involved analyses of chemical composition followed by trial refinements of the most apparent, common phases; and usage of automatic phase recognition software (e.g. Panalytical HighScore 3.0) to search for secondary phases and to confirm the main phases. The resolution of the instrument calibrated using the NIST 660 standard is 0.065° of 2θ, which is significantly below the widths of lines in samples. The data were collected with an angular step of 0.016° of 2θ. The calibration measurements using NIST 660 revealed also instrumental broadening of the collected lines, which is essential for further analyses of reflection profiles.

3 Results and discussion

3.1 General description and mineral composition of the magnetic fraction

After 9 months of exposure, the surfaces of the sampler were covered with a thin and uneven layer of dust (Fig. 2).

The magnetic fraction collected on the sampler surfaces is composed of grainy material of different size and colour. The dominant part of the grains is dark grey, although colourless and transparent, brown, reddish or lustrous are also present (Fig. 2c). The size of the particles observed by electron microscopy varies from more than 30 µm to below 100 nm. The number of the largest particles in the sample is low, but their share is significant considering the volume or mass of these particles. Because of the relatively high content of particles larger than 10 µm, the sample differs from typical PM_{10} samples.

The results of the XRD studies (Fig. 3) suggest that the separated fraction is dominated by magnetite (27.9 wt %), hematite (14.8 wt %) and α-Fe (1.5 wt %) in terms of the magnetic phases. It also exhibits quartz (41.2 wt %), feldspar (10.0 wt %) and pyroxene (4.6 wt %). Quartz grains observed using SEM are angular and differ in size (with the largest up to 50 µm). Angular grains with chemical composition similar to K-feldspar and usually platy Ca sulphate crystals (possibly gypsum) were also noted using the SEM-EDS method.

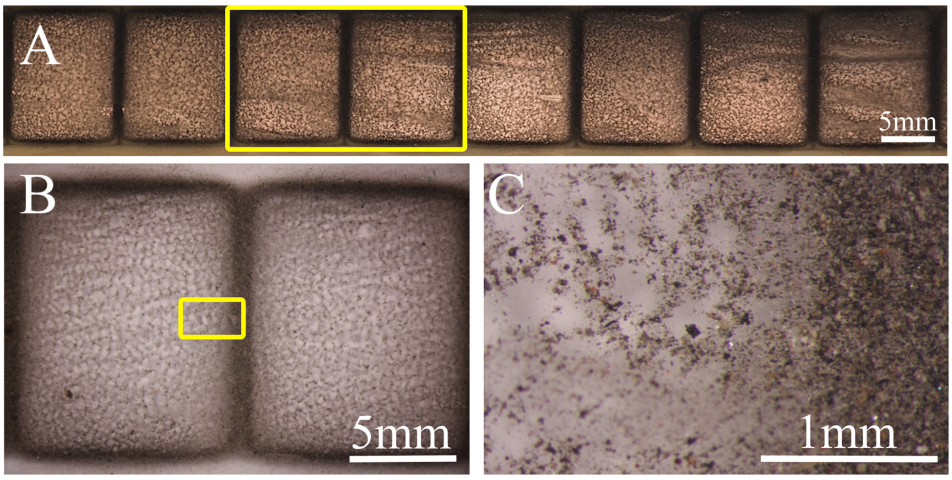

Figure 2. Magnetic fraction on the passive sampler after 9 months of deposition. **(a, b, c)** Sample of the surface of rectangular magnet covered with PVC foil with dust grains of various colour, size and shape on the surface of the sampler. **(c)** and **(b)** are zoomed-in areas of the yellow rectangular areas in **(a)** and **(b)** respectively.

Relatively common are grains containing Fe, Si, Al, Ca and other elements (possibly aluminosilicates).

A precise analysis of the profile of magnetite reflections in the XRD pattern suggest the distribution of various elements at the Fe sites (e.g. Cr, Mn, Co, Zn) as typical of naturally abundant ferrites (Fig. 3), as evidenced by a strain in the profile of this phase. The strain can be extracted from instrumental broadening (thanks to calibration measurements), and therefore Rietveld refinement revealed strains for all phases. The residual strains are related to static defects of the structure, e.g. atomic disorder on Wyckoff positions originating from substitution of different types of atoms into specific sites. The refined strain was found to be about 0.75 %, which is significantly higher than typical values for pure Fe_3O_4 specimens, which is smaller than 0.2 % (the pure Fe_3O_4 specimen was also measured as a reference). The resulting broadening of the main reflections of the Fe_3O_4 (220 at 30.1° of 2θ and 311 at 35.5° of 2θ) can be noted in the insets of Fig. 3.

3.2 Form of occurrence of Fe-containing particles

Fe-containing particles analysed using the SEM-EDS method differ in size and morphology. Both irregular and spherical particles are present (Fig. 4a). The spherical particles are considered to be of anthropogenic origin and related to high-temperature processes. The occurrence of natural spherical particles (cosmic, volcanic, lightning induced; e.g. Genareau et al., 2015; Genge et al., 2017a) is very limited in comparison with the anthropogenic ones, but it is not possible to exclude the occurrence of spherical micrometeorites in the dust collected in urban environments (Genge et al., 2017b). In the atmospheric particulate matter studied by Ebert et al. (2000) and Choël et al. (2007), most of the Fe-rich particles were spherical, that is anthropogenic in origin. In the magnetic fraction collected in Kraków, irregular angular particles significantly prevail over spherical ones (especially in the more coarse-grained fractions), taking into account the number of particles. In the case of irregular particles, the distinction between natural and anthropogenic is difficult.

Fe-containing particles occur as discrete forms of diverse size and morphology (Fig. 4a, b). Numerous Fe-containing particles occur as grains attached to the surface of larger grains (e.g. quartz, feldspar, various aluminosilicates, gypsum, spherical particles of various composition and pollen grains) (Fig. 4b–d). The number of Fe-containing particles attached to the aforementioned larger grains varies greatly. This form of occurrence of the atmospheric dust can be considered as an example of heterogenous clustering (Pietrodangelo et al., 2014).

Fe-containing particles also occur as a component of aggregates of various sizes and morphologies (Fig. 4e and f). The size and composition of the particles in aggregates are differentiated. Aggregates of larger particles are heterogenous (heterogenous clustering; Pietrodangelo et al., 2014). Homogeneous aggregates (homogeneous clustering; Pietrodangelo et al., 2014) are usually composed of small (below 200 nm) Fe-rich spheres (Fig. 4g and h). Magnetic Fe-containing particles attached to larger grains or present in aggregates cause the accumulation of quartz, feldspars and other non-magnetic components in the magnetic fraction, as evidenced by XRD.

3.3 Size, morphology and chemical composition of Fe-rich particles

The Fe-containing particles vary in size from over 20 µm (rarely) (Fig. 5a and b) to nanoparticles below 100 nm (Fig. 4g, h). The particles are irregular in shape, sometimes

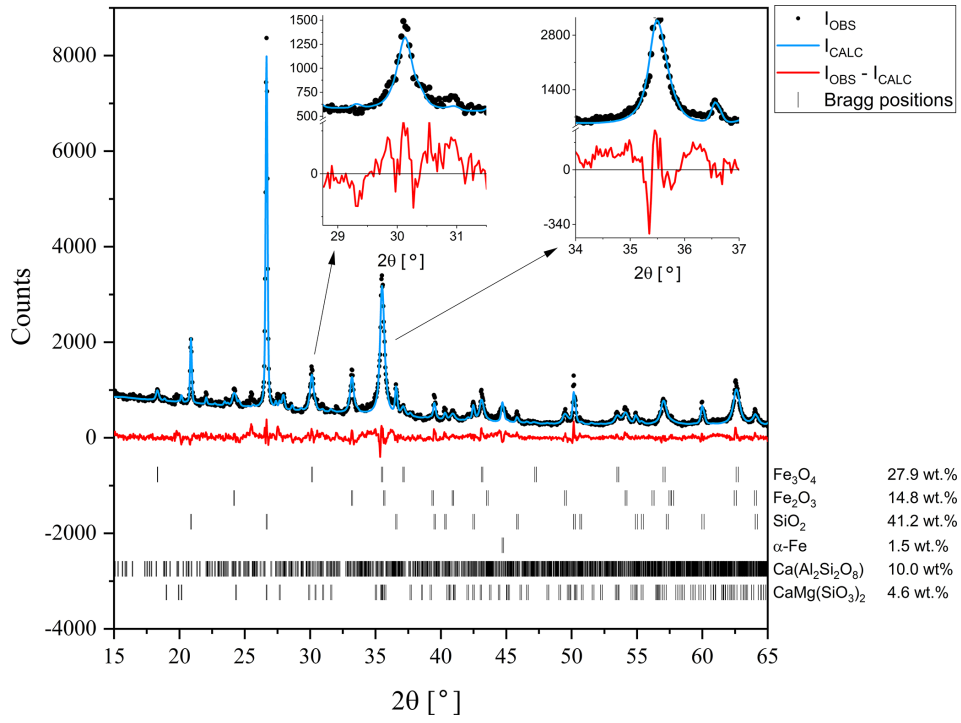

Figure 3. X-ray diffraction pattern measured at room temperature. The black circles stand for measured data, the blue line represents calculated spectra obtained assuming material composition as indicated, and the red line denotes the difference between the observed and calculated intensities. Calculated positions of the diffraction peaks for each phase are indicated as bars.

angular, or spherical (Figs. 4a, 5a–d). The content of the spherical particles in fractions over 10, 10–5, 5–2.5 and 2.5–1 µm is variable and significantly lower than the irregular ones. In the fraction below 1 µm, the number of spherical particles (53 %) slightly dominates the irregular ones. The results of the chemical analyses of 278 Fe-containing particles (see Table S1 in file "Supplement B" in the Supplement for a complete list of results) indicate that the Fe content varies from 2.32 wt % to 98.18 wt %. Particles with lower content of Fe are usually enriched in Si and Al. For some of them, the chemical composition corresponds to pyroxenes determined using XRD analysis. Trace elements (content below 0.1 wt %) noted in single particles are not discussed because of insufficient statistical significance of these results.

Numerous irregular Fe-based particles contain Cr (up to 28 wt %), Zn (up to 19 wt %), Mn (up to 11 wt %) and Cu (up to 7.5 wt %) (Fig. 5h). Ni (up to 8 wt %) occurs rarely, and exclusively in particles containing Cr. W and V occur rarely in the irregular Fe-rich particles, usually in low amounts (W up to 5.45 wt %, V up to 0.76 wt %). Sb and Sn were noted only in a few particles (up to ca. 1.5 wt %). Determination of the origin of the Fe-containing particles is difficult. According to Bogacki et al. (2018) re-entrained road dust contributes to 25 % in winter and 50 % in summer of the PM_{10} in the air in selected streets in the centre of Kraków. It indicates that long-lasting, multi-stage evolution and mixing of atmospheric particulate is possible. The form of occurrence (irregular) can be related both to natural sources (e.g. soils and the disintegration of rocks) or anthropogenic sources (e.g. metallurgical industry, fuel combustion, other industrial sectors, and traffic-related sources such as exhaust and non-exhaust emissions).

According to Li et al. (2021), Fe and steel production is a main source of magnetic particle emissions, while emissions from power plants come in second place. It can be assumed that for the irregular particles studied, a natural origin is less probable, especially for the larger particles where the range of transportation in the atmosphere is limited. However, taking into account their abundance in the atmospheric particulate matter samples and the scarcity of their possible natural sources in the study area, it is possible to assume that the dominant part is of anthropogenic origin. The chemical composition can be considered as an important indication of the origin of Fe-rich airborne particles (cf. Wilczyńska-Michalik et al., 2020b). It is often assumed that anthropogenic Fe-rich particles are mostly spherical (e.g. Choël et al., 2007). This is the common form originating from high-temperature processes, but in Fe metallurgy dust of different shape, size and chemical composition can be emitted (Jarzębski and Kapała, 1975; Wilczyńska-Michalik, 1981; Jabłońska et al., 2021). In 1979 steelworks in Kraków alone emitted dust containing 18 000 t of Fe (Cole, 1991). In 1985 the emission of Fe in dust in the Kraków region was estimated to be 14 000 t (Helios Rybicka, 1996). Recently the emission of Fe-rich dust

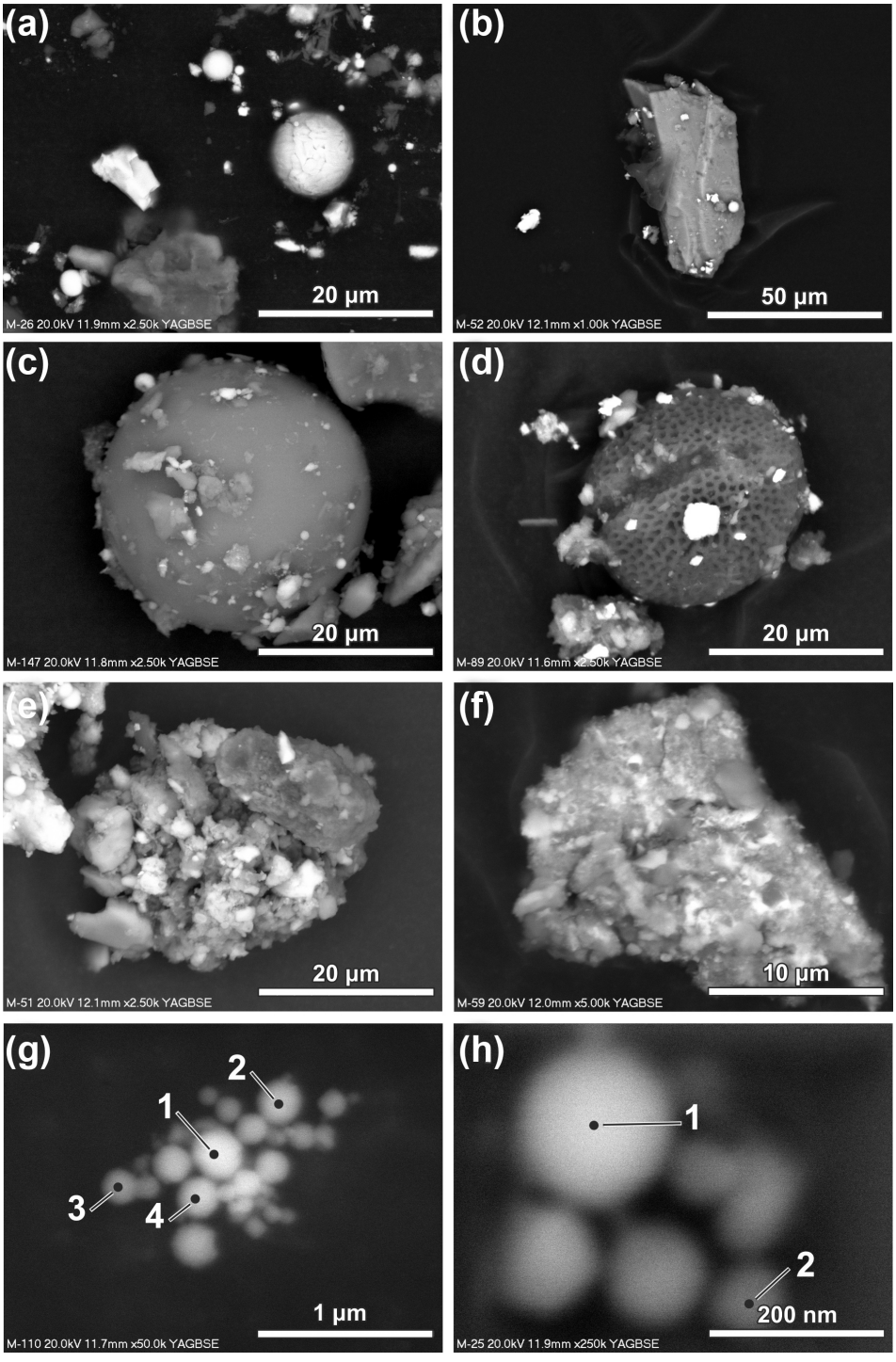

Figure 4. Forms of occurrence of magnetic particles (SEM; backscattered electron images). **(a)** Discrete particles of different size and shape. **(b)** Ca-rich aluminosilicate grain with attached magnetic particles. **(c)** Aluminosilicate sphere with attached magnetic particles. **(d)** Pollen grain with attached magnetic particles. **(e)** Aggregate of angular aluminosilicate grains of various chemical composition and Fe-rich particles. **(f)** Aggregate of fine particles often with diffused boundaries; bright particles are Fe-rich. **(g)** Aggregate composed of spherical Fe-rich particles below 200 nm in size. **(h)** Aggregate composed of spherical Fe-rich particles below 200 nm in size (see Table 1 for the results of the chemical composition measurements of the indicated particles).

from Fe metallurgy is significantly lower but this emission is still present. It is also likely that irregular Fe-containing particles are derived from fragmented metallurgical slags that show a variety of chemical and mineral compositions, but often contain Fe-rich components (Neuhold et al., 2019; Potysz and Kierczak, 2019), and also Cr and Mn (Horckmans et al., 2019). Metallurgical slags are often used as a substitute of natural aggregate (Horckmans et al., 2019), which could be a reason for the broad dispersion of slag-derived dust in the atmosphere. Irregular Fe-rich particles are also related to rail transportation (Moreno et al., 2015). Most of the Fe-rich particles described in the literature from this source are composed of hematite. The sampling site was situated ca. 250 m from two tram stops, which indicates that this source could also contribute to the collected magnetic fraction. Fe-rich particles occur commonly in road dust and their origin can be related to non-exhaust traffic emissions such as brake-wear emission (Grigoratos and Martini, 2015).

Several types of spherical Fe-rich particles were noted in the magnetic fraction (Fig. 5c). Aluminosilicate spheres containing usually 5 wt %–20 wt % of Fe occur rarely (Fig. 4c). Production of energy in coal-fired power plants can be considered as the main source of particulate matter of this type (Wilczyńska-Michalik et al., 2020a). Spherical forms with Fe content within the range of 35 wt %–60 wt % and Si in the 15 wt %–35 wt % range are not numerous. Only one Fe-rich spherical particle with relatively high content of Ca (possibly calcium ferrite) was noted (Fig. 4d). Oxides of Fe_xO_y type strongly dominate the group of spherical particles. Most of these particles can be attributed to the industrial metallurgical processes (e.g. Choël et al., 2007). Spherical particles containing Cr are rare. Zn is also rare in the Fe oxide spherical particles with a diameter larger than 1 µm.

Most of the spherical particles below 1 µm contain Zn (up to 27.8 wt %) (Fig. 4h, h). This can be related to the deposition of Zn on the surfaces of small particles during the cooling of volatile substances from metallurgical processes (Ebert et al., 2000). Mn is also a common element in Fe-rich spherical particles below 1 µm in diameter, with the highest content around 10 wt %. Cr occurs relatively rarely in this group of spherical particles. Spherical particles below 200 nm are relatively common in the group of particles below 1 µm. Spherical Fe-rich particles below 1 µm in diameter are commonly formed in metallurgical processes (Jenkins, 2003; Jenkins and Eagar, 2005). Spherical Fe nanoparticles derived from the in-cylinder melting of metallic engine parts contain Mn and Cr (Liati et al., 2015). Rail transport was recognized as a possible source of spherical nanoparticle aggregates composed of magnetite (Moreno et al., 2015). Spherical forms of 500 nm usually occur in clusters.

In the magnetic fraction, particles with high content of other metals or dominated by metals other than Fe occur rarely (Fig. 5e, f, g, h). A few particles rich in Pb were noted (up to 70 wt %) (Fig. 5e). Three irregular particles below 1 µm in size devoid of Fe and composed predominately of Zr and O (two particles) (Fig. 5f) or Au (Fig. 5g) were analysed.

S is commonly noted in the Fe-rich particles studied and is often accompanied by Na (Fig. 4h), Cl, K, Ca, Mg and Ba. It was noted by Ito et al. (2018) that Fe in aged fly ashes is coated by Fe sulphates. According to Li et al. (2016), atmospheric metal particles are internally mixed with secondary sulphates or other components.

A few particles are relatively rich in S and Fe, but without any measured O content that can indicate the presence of a sulphide component.

TEM investigations were aimed at the characterization of the smallest fraction of the analysed atmospheric dust samples. Figure 6 presents examples of bright-field TEM images of the studied material. The observed particles vary widely in size and shape. The smallest particles observed are well below 10 nm in size, with the large ones exceeding a few hundred nanometres. Irregular morphology is predominant regardless of the particle size (Fig. 6a, e, f, g). Nevertheless, spherical particles of 50–200 nm diameter were also observed (Fig. 6a, b, c, d). Most of the particles analysed using EDS are rich in Fe and O, while some of them also contain Si, Zn, Mn, Al or Mg.

SAED collected from an agglomerate of the smallest fraction particles (Fig. 6e, f) enabled the determination of the presence of magnetite (JCPDS card no. 00-001-1111), which is consistent with the XRD analysis performed. Domains with the magnetite ordering reach the size of 10 nm (Fig. 6g, h).

HRTEM imaging made it possible to prove the existence of the ferrous nanoparticles below 10 nm in diameter on one hand and bigger – up to 200 nm – on the other. Moreover, we clearly show the crystallinity of these smallest particles proving their chemical composition, which is important information for assessing their impact on human health.

3.4 Mössbauer spectroscopy

Experimental data collected at room temperature and at 80 K were refined using doublet and sextet components (Fig. 7) based on the composition of the samples obtained on the basis of XRD and chemical analysis, as well as the available data from the literature. For the analysis of the results, isomer shift (IS), quadrupole splitting (QS, defined as half of the distance between the doublet peaks in our fits) and hyperfine magnetic field (B) were taken into account, together with the relative intensity (rel. int.) of each component. One has to keep in mind that in the case of the material under investigation, we cannot dismiss the possibility of the particles being of non-stoichiometric composition, having a large number of defects and finally their surfaces being affected by atmospheric conditions.

At room temperature, satisfactory results are obtained using two doublet contributions and three magnetically split sextets. The former are attributed to $(Ca,Mg,Fe)(SiO_3)_2$

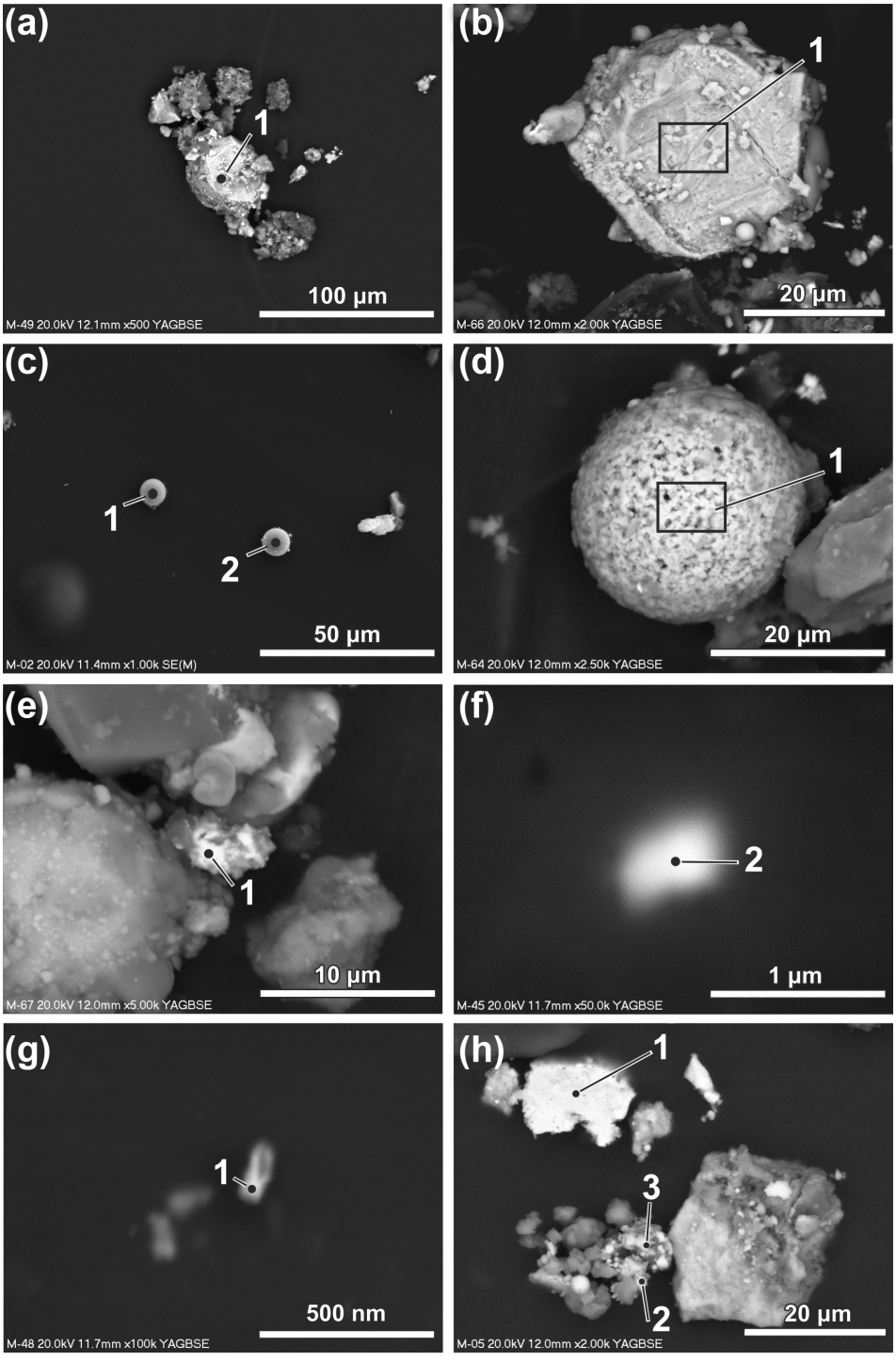

Figure 5. Size and morphology of Fe-rich particles and particles dominated by metals other than Fe or with high content of other elements (SEM; backscattered electron images except **c** – secondary electrons). **(a)** Irregular particles larger than 20 µm. **(b)** Irregular particles larger than 20 µm. **(c)** Aluminosilicate sphere (left) and Fe-dominated sphere (right). **(d)** Spherical particle rich in Ca and Fe. **(e)** Particle rich in Pb. **(f)** Particle rich in Zr. **(g)** Particle rich in Au. **(h)** Particles with high content of metals other than Fe (see Table 1 for the results of the chemical composition measurements of the indicated particles).

Table 1. Results of chemical analyses for spots or areas marked in Figs. 4 and 5 (empty fields – elements not determined).

Figure	Spot or area	Element (wt %)																			
		Fe	Mn	Cr	Ni	Zn	W	Pb	Au	Zr	Ti	Si	Al.	P	O	S	Ca	Mg	K	Na	Cl
4G	1	60.04				14.66						3.23	1.58		16.27	3.40	0.82				
	2	62.96				3.59						3.13	0.90		17.95	3.78	1.17			6.52	
	3	59.38	1.35			4.41						3.75	1.47		18.24	4.93	1.40			5.07	
	4	60.19				11.67						3.85	1.74		17.53	4.04	0.98				
4H	1	62.06				3.95						2.83			17.29	6.29				7.58	
	2	46.52										5.84			19.89	13.06				14.69	
5A	1	98.18										0.50			0.82		0.34			0.16	
5B	1	91.33	0.46									0.56			7.12		0.53				
5C	1	4.85									1.07	35.37	18.60		31.23		0.54	1.79	5.00	1.55	
	2	87.55										0.26		0.13	12.06						
5D	1	40.01	2.89			1.47					0.70	2.32	1.95	0.13	14.37	0.15	35.57	0.31			0.13
5E	1	3.74					2.31	70.25							11.89	10.32	1.49				
5F	1									73.08					21.41	3.64				1.87	
5G	1								85.71			4.05			0.10					10.24	
5H	1	68.34	5.74	12.44	6.33							3.34	0.22		2.72	0.49	0.38				
	2	55.64	4.15	0.87		13.61						4.06	2.32		12.93	2.22	2.64	1.56			
	3	44.85	8.56	1.26	1.08	19.78					0.16	2.78	0.97		12.70	1.19	3.37	2.91			0.39

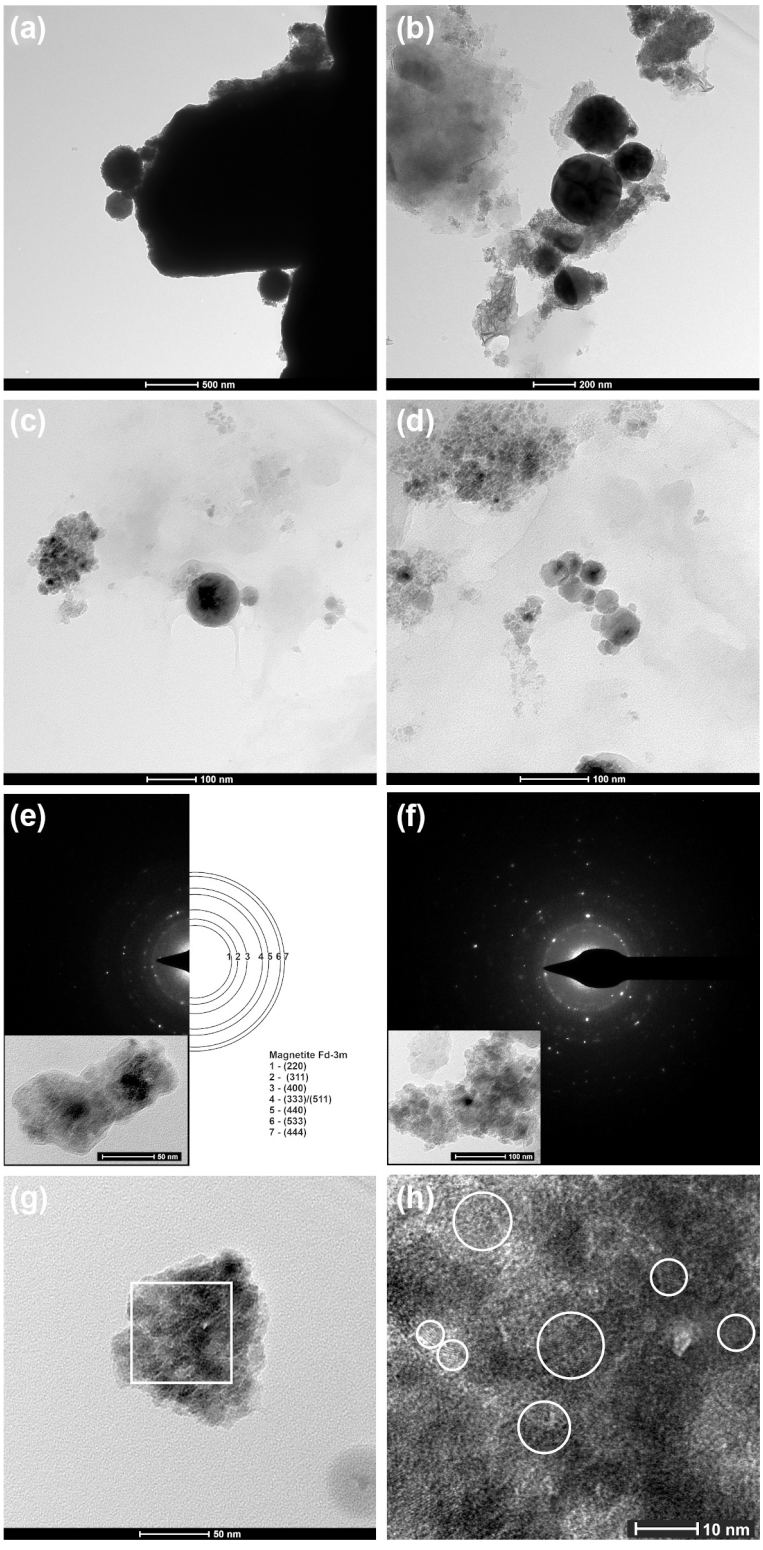

Figure 6. Fe- rich particles (TEM studies). **(a)** Large spherical and irregular particles rich in Fe **(b, c, d)**. Spherical particles of various size rich in Fe **(e, f)**. SAED analyses of aggregates of irregular Fe-rich particles (particles shown in insets). **(g)** Aggregate of Fe rich-particles. White square – area of HRTEM analysis. **(h)** HRTEM analysis; white circles – domains with visible magnetite ordering.

(20.3 %) and to a collapsed spectra of FeO_x (32.2 %). The sextet due to a hyperfine magnetic field can be ascribed to the presence of α-Fe_2O_3 (18.9 %), large Fe_3O_4 (32.4 %) grains and bigger particles, as well as FeX alloy (5.3 %). Low-temperature measurements further support our predictions made on the basis of the room temperature measurements showing again two quadrupole split contributions: $(Ca,Mg,Fe)(SiO_3)_2$ (20.2 %) and superparamagnetic Fe/Fe oxide particles. Three magnetically split components are again related to FeX alloy 7.4 %), α-Fe_2O_3 (10.1 %) and Fe_3O_4 grains (35.6 %). As can be seen in Table 2, the contribution from Fe_3O_4 changes from two to four sextets. This is due to the fact that in Fe_3O_4, the Fe cations occupy two inequivalent crystallographic positions: tetrahedral (T) and octahedral (O) sites (Tong et al., 2001). Therefore, the spectrum of Fe_3O_4 at room temperature (well above the Verwey transition – 120 K) is composed of only two sextets corresponding to Fe^{3+} cations on a T site, and to Fe^{2+}/Fe^{3+} cations on an O site. Below 120 K, the relaxation time is extended and, consequently, the O sites occupied by Fe^{2+} and Fe^{3+} can be differentiated (Řezníček et al., 2017).

Interestingly, the contribution of the superparamagnetic particles is significantly diminished (falling from 24 % at room temperature to less than 5 % at 80 K). At the expense of the doublet component, a new magnetically split contribution arises related to tiny Fe_3O_4-like particles giving about 22 % of the spectra. Such behaviour of the Mössbauer spectrum typically belongs to nanosized ferromagnetic or antiferromagnetic particles. Such particles (of the sizes below a single domain boundary) will present reduced hyperfine fields owing to spin relaxation effects (Yamada and Nishida, 2019). Our Mössbauer spectroscopy results indicate that Fe-bearing particles in the aerosols are very small, showing a superparamagnetic behaviour at room temperature (RT) and becoming ferromagnetic while lowering the measurement temperature. On one hand, the possibility of superparamagnetic particles being present in the suspended particulate matter was dismissed by some authors on the basis of the magnetization measurements (Magiera et al., 2021). On the other hand, the possibility of the long-range transportation of tiny (a few nanometres to a few tenths of a nanometre in diameter) particles far from the industrial sources cannot be eliminated. Moreover, such particles will not only travel over large distances, but also stay suspended for a long time. Our results are also in agreement with those presented by other groups studying aerosols and suspended particulate matter (Fu et al., 2012; Muxworthy et al., 2003).

The presence of some amount of aluminosilicates cannot be dismissed based on the existence of a small component that is not magnetically split down to 80 K; however, the IS values do not fully support this statement, at least for ideal chemical composition and crystalline structure.

We are also aware of the possibility of Fe^{3+}/Fe^{2+}-containing glasses to be used for Mössbauer spectra interpretation in the case of coal combustion products (Huffman et al., 1981; Murad and Cashion, 2004). These are commonly found in ashes from high-temperature processes (their content becoming larger as the combustion temperature rise) and are identified on the basis of the QS / IS ratio as they show a sextet collapsed into a doublet with very broad lines. Taking into account the way we collected our samples, we would rather dismiss ferric or ferrous glasses from being present in the material under investigation.

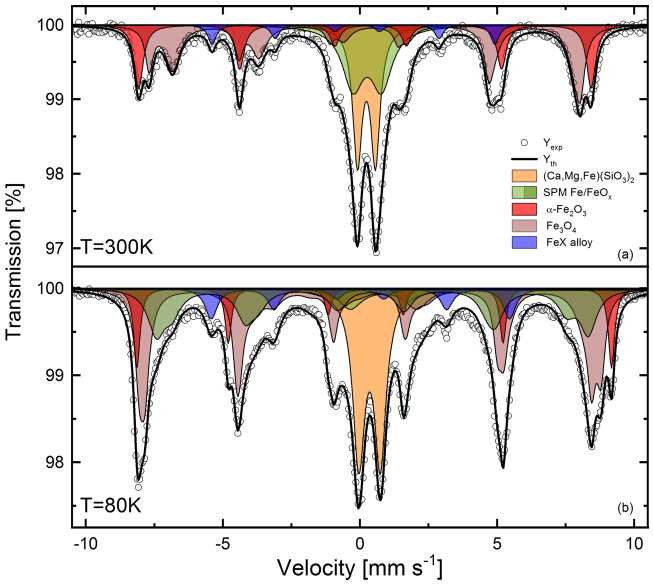

Figure 7. Mössbauer spectra measured at room temperature **(a)** and at 80 K **(b)**. For a detailed explanation and the hyperfine interaction parameter of the components used for fitting the spectra, see the text and Table 2.

3.5 Magnetization (VSM) measurements

Magnetization (VSM) measurements of the magnetic fraction were performed between 295 and 77 K. The sample shows typical ferromagnetic behaviour (Fig. 8). The material is almost fully saturated both at high and low temperatures. At 77 K, a wider hysteresis loop is observed as compared to the RT measurements. The widening of the hysteresis loop could be associated with blocking of superparamagnetic particles at low temperatures. Typically, a well-defined maximum in the ZFC curve is associated with the blocking temperature of superparamagnetic nanoparticles of well-defined size. However, for the broad distribution of nanoparticle sizes such a maximum is usually not observed. This is apparently our case, as the ZFC curve shows no maximum but a constant increase up to the RT.

In our recent contribution (Wilczyńska-Michalik et al., 2020b), the results of both magnetic and Mössbauer spectroscopy studies of the soil samples from sites at different distances from sources of industrial pollution were presented. The magnetometric data previously reported for the

Table 2. Hyperfine interaction parameters (isomer shift, quadrupole splitting, hyperfine magnetic field) and relative component contribution for samples measured at room temperature (300 K) and low temperature (80 K) (IS with respect to metallic Fe at 300 K).

Component	Temperature [K]	Rel. Contr. [%]	IS [mm s^{-1}]	B [kGs]	QS [mm s^{-1}]
α-Fe_2O_3	300	18.9	0.389	511.4	−0.105
	80	10.1	0.4678	536.4	0.156
Fe_3O_4	300	32.4	0.264	487.5	0.018
			0.645	455.4	−0.026
	80	35.6	0.479	521.5	0
			0.4082	504.8	0
			0.5446	496.1	−0.325
			0.978	393.0	1.219
FeX alloy	300	5.3	−0.065	319.6	−0.067
	80	7.4	0.1179	337.1	0
$(Ca,Mg,Fe)(SiO_3)_2$	300	20.3	0.341		0.327
	80	20.2	0.4549		0.393
SPM Fe / FeO_x	300	20.3	0.369		0.522
		2.9	1. 258		0.35
	80	22	0.518	488.1	0.037
			0.5096	446.0	−0.060
		4.7	0.9662		1.212

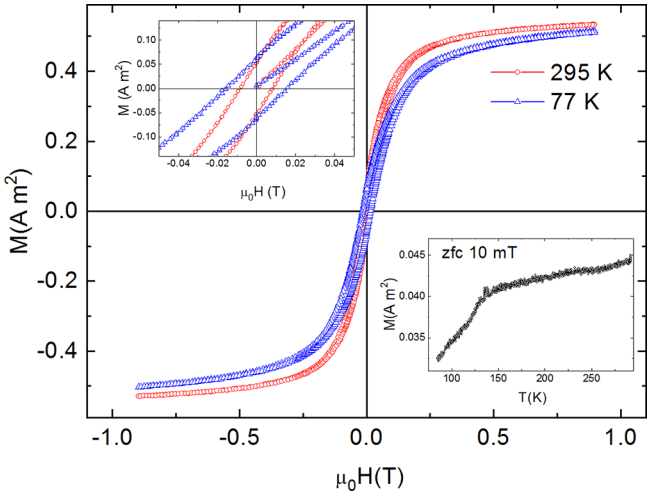

Figure 8. Magnetic hysteresis loops up to 0.9 T at room temperature (red) and at 77 K (blue). Top-left inset: close-up of the area close to the zero field. Bottom-right inset: ZFC curve between 300 and 77 K.

soils show a high degree of similarity to the currently discussed samples. In the case of Mössbauer spectroscopy, the situation becomes more complicated as the soil samples certainly undergo diverse processes due to oxygen exposure, humidity and so forth. However, we still observe that the fingerprints of anthropogenic particles found in our present study are clearly recognized in soils from polluted areas, in sharp contrast to soil samples from sites far from industrial plants.

3.6 Possible environmental and health impact of Fe-rich particles

Although the direct environmental and health impact was not studied, it can be suggested that both the high abundance of Fe-rich particles and the form of their occurrence (high content of nanoparticles) indicate potential threat. Finely dispersed Fe and other transition metal-rich particles from various sources (e.g. combustion, friction, industrial emission, crustal material, road dust) are considered to have a negative impact on human health (Lodovici and Bigagli, 2011; Maher et al., 2016; Calderón-Garcidueñas et al., 2019; Gonet and Maher, 2019; Maher, 2019; Maher et al., 2020; Shahpoury et al., 2021; Hammond et al., 2022).

Fe and other transition metal-rich particles (especially when finely dispersed) can be active in reactions occurring in the atmosphere, e.g. in the catalytic oxidation of SO_2 in the atmosphere and the formation of sulphate aerosol (Alexander et al., 2009; Dupart et al., 2012) or the formation of brown carbon particles (e.g. Al-Abadleh, 2021).

A high content of anthropogenic Fe-rich particles in the studied material related to fuel combustion or other high-temperature processes can suggest relatively high bioavailability of Fe (e.g. Ito et al., 2019, 2021b). Determination of the wide span in the size of Fe-rich particles resulting from our study is also important taking into account their different potential reactivity (Liu et al., 2022).

Fe-rich, airborne particles participate in the heating effect of the atmosphere (Moteki et al., 2017; Ito et al., 2018) and they impact on climate change. It is important to emphasize

the effect of the size of these particles and their role in heating (Ito et al., 2021a).

4 Conclusions

- Magnetic components are present as discrete particles, as particles attached to larger grains or in aggregates of various size and composition.
- Fe-rich magnetic particles differ in morphology (irregular or spherical) and size (from over 20 µm to nanoparticles well below 100 nm). Apart from Fe, other metals are also present in these particles.
- Spherical particles formed in high-temperature processes are of anthropogenic origin. Most of the irregular particles are probably also of anthropogenic origin, but natural sources could also be considered.
- The abundance of spherical particles is higher among smaller particles. Spherical Fe-rich particles below 200 nm in size (often containing Zn and other metals) are a characteristic component occurring often as homogeneous aggregates.
- The results of the XRD studies suggest that the separated fraction is dominated by magnetite, hematite and α-Fe in terms of the magnetic phases. It also exhibits quartz, feldspar and pyroxene.
- Mössbauer spectroscopy indicates the presence of Fe_3O_4, α-Fe_2O_3, metallic Fe (FeX alloy) and $(Ca,Mg,Fe)(SiO_3)_2$. Clear evidence of the occurrence of nanometre-scale Fe_3O_4 particles was shown.
- The study of a larger number of samples will offer a better understanding of the range of variability of the material as well as of the impact on health and on the environmental.
- Results indicate that the Fe particles analysed can impact human health and the environment in multiple ways in urbanized areas.
- Studying samples obtained directly at the emission sources and their comparison with our present results could give an indication of the impact of the particular industrial activities on the environment.

Data availability. The data that support the findings of this study are available from the corresponding author, Jan M. Michalik, upon request.

Supplement. The supplement related to this article is available online at: https://doi.org/10.5194/acp-23-1449-2023-supplement.

Author contributions. JMM developed the concept, formulated the research as well as the goals and aims of the research, supervised the research, verified the results, analysed the experimental data, prepared the visualization of the data and wrote the original draft. All the authors contributed to the investigation. ŁG, JŻ, WWM and MM participated in intense discussions as well as in reviewing and editing the final version of the manuscript.

Competing interests. The contact author has declared that none of the authors has any competing interests.

Disclaimer. Publisher's note: Copernicus Publications remains neutral with regard to jurisdictional claims in published maps and institutional affiliations.

Acknowledgements. The authors are grateful to Waldemar Obcowski for his help in the preparation of some of the figures.

Financial support. The Ministry of Science and Higher Education and the Faculty of Physics and Applied Computer Science AGH UST statutory tasks (Łukasz Gondek, Jan M. Michalik, Waldemar Tokarz and Jan Żukrowsk), the Faculty of Geography and Biology at the Pedagogical University of Kraków (Wanda Wilczyńska-Michalik), and the Faculty of Geography and Geology at Jagiellonian University (Marek Michalik) funded this research. The study was included in "The Anthropocene as the Epoch of Natural Environment Transformation" project at the Pedagogical University. At Jagiellonian University, the study was performed within the "Anthropocene" Priority Research Area under the "Excellence Initiative – Research University" programme. Jan M. Michalik acknowledges partial support by the National Science Centre in the framework of the MINIATURA 5 founding (grant no.: UMO-2021/05/X/ST10/00975).

Review statement. This paper was edited by Markus Ammann and reviewed by three anonymous referees.

References

Al-Abadleh, H. A.: Aging of atmospheric aerosols and the role of iron in catalyzing brown carbon formation, Environ. Sci. Atmos., 1, 297–345, https://doi.org/10.1039/D1EA00038A, 2021.

Alexander, B., Park, R. J., Jacob, D. J., and Gong, S.: Transition metal-catalyzed oxidation of atmospheric sulfur: Global implications for the sulfur budget, J. Geophys. Res., 114, D02309, https://doi.org/10.1029/2008JD010486, 2009.

Baatar, A., Ha, R., and Yu, Y.: Do rainfalls wash out anthropogenic airborne magnetic particulates? Environ. Sci. Pollut. Res., 24, 9713–9722, https://doi.org/10.1007/s11356-017-8638-9, 2017.

Baker, A. R., French, M., and Linge, K. L.: Trends in aerosol nutrient solubility along a west–east transect of the Saharan dust plume, Geophys. Res. Lett., 33, L07805, https://doi.org/10.1029/2005GL024764, 2006.

Biswas, P. and Wu, C.-Y.: Nanoparticles and the Environment, J. Air Waste Manage., 55, 708–746, https://doi.org/10.1080/10473289.2005.10464656, 2005.

Bogacki, M., Mazur, M., Oleniacz, R., Rzeszutek, M., and Szulecka, A.: Re-entrained road dust PM_{10} emission from selected streets of Krakow and its impact on air quality, Air Protection in Theory and Practice, E3S Web Conf., 28, 01003, https://doi.org/10.1051/e3sconf/20182801003, 2018.

Buck, C. S., Landing, W. M., and Resing, J. A.: Particle size and aerosol iron solubility: A high-resolution analysis of Atlantic aerosols, Mar. Chem., 120, 14–24, https://doi.org/10.1016/j.marchem.2008.11.002, 2010.

Calderón-Garcidueñas, L., González-Maciel, A., Mukherjee, P. S., Reynoso-Robles, R., Pérez-Guillé, B., Gayosso-Chávez, C., Torres-Jardón, R., Cross, J. V., Ahmed, I. A. M., Karloukovski, V. V., and Maher, B. A.: Combustion- and friction-derived magnetic air pollution nanoparticles in human hearts, Environ. Res., 176, 108567, https://doi.org/10.1016/j.envres.2019.108567, 2019.

Cheng, M.-D., Allman, S. L., Ludtka, G. M., and Avens, L. R.: Collection of airborne particles by a high-gradient permanent magnetic method, J. Aerosol Sci., 77, 1–9, https://doi.org/10.1016/j.jaerosci.2014.07.002, 2014.

Cheng, M.-D., Murphy, B. L., Moon, J.-W., Lutdka, G. M., and Cable-Dunlap, P. R.: On the use of high-gradient magnetic force field in capturing airborne particles, J. Aerosol Sci., 120, 22–31, https://doi.org/10.1016/j.jaerosci.2018.03.007, 2018.

Choël, M., Deboudt, K., Flament, P., Aimoz, L., and Mériaux, X.: Single-particle analysis of atmospheric aerosols at Cape Gris-Nez, English Channel: Influence of steel works on iron apportionment, Atmos. Environ., 41, 2820–2830, https://doi.org/10.1016/j.atmosenv.2006.11.038, 2007.

Cole, D. H.: Cleaning Up Krakow: Poland's Ecological Crisis and the Political Economy of International Environmental Assistance, Articles by Maurer Faculty, Paper 724, http://www.repository.law.indiana.edu/facpub/724 (last access: 10 January 2023), 1991.

Dupart, Y., King, S. M., Nekat, B., Nowak, A., Wiedensohler, A., Herrmann, H., David, G., Thomas, B., Miffre, A., Rairoux, P., D'Anna, B., and George, C.: Mineral dust photochemistry induces nucleation events in the presence of SO_2, P. Natl. Acad. Sci. USA, 109, 20842–20847, https://doi.org/10.1073/pnas.1212297109, 2012.

Ebert, M., Weinbruch, S., Hoffmann, P., and Ortner, H. M.: Chemical Characterization of North Sea Aerosol Particles, J. Aerosol Sci., 31, 613–632, https://doi.org/10.1016/S0021-8502(99)00549-2, 2000.

Fu, H., Lin, J., Shang, G., Dong, W., Grassian, V. H., Carmichael, G. R., Li, Y., and Chen, J.: Solubility of Iron from Combustion Source Particles in Acidic Media Linked to Iron Speciation, Environ. Sci. Technol., 46, 11119–11127, https://doi.org/10.1021/es302558m, 2012.

Genareau, K., Wardman, J. B., Wilson, T. M., McNutt, S. R., and Izbekov, P.: Lightning-induced volcanic spherules, Geology, 43, 319–322, https://doi.org/10.1130/G36255.1, 2015.

Genge, M. J., Davies, B., Suttle, M. D., van Ginneken, M., and Tomkins, A. G.: The mineralogy and petrology of I-type cosmic spherules: Implications for their sources, origins and identification in sedimentary rocks, Geochim. Cosmochim. Ac., 218, 167–200, https://doi.org/10.1016/j.gca.2017.09.004, 2017a.

Genge, M. J., Larsen, J., Van Ginneken, M., and Suttle, M. D.: An urban collection of modern-day large micrometeorites: Evidence for variations in the extraterrestrial dust flux through the Quaternary, Geology, 45, 119–122, https://doi.org/10.1130/G38352.1, 2017b.

Gonet, T. and Maher, B. A.: Airborne, Vehicle-Derived Fe-Bearing Nanoparticles in the Urban Environment: A Review, Environ. Sci. Technol., 53, 9970–9991, https://doi.org/10.1021/acs.est.9b01505, 2019.

Górka-Kostrubiec, B., Magiera, T., Dudzisz, K., Dytłow, S., Wawer, M., and Winkler, A.: Integrated Magnetic Analyses for the Discrimination of Urban and Industrial Dusts, Minerals, 10, 1056, https://doi.org/10.3390/min10121056, 2020.

Grigoratos, T. and Martini, G.: Brake wear particle emissions: a review, Environ. Sci. Pollut. Res., 22, 2491–2504, https://doi.org/10.1007/s11356-014-3696-8, 2015.

Hammond, J., Maher, B. A., Gonet, T., Bautista, F., and Allsop, D.: Oxidative Stress, Cytotoxic and Inflammatory Effects of Urban Ultrafine Road-Deposited Dust from the UK and Mexico in Human Epithelial Lung (Calu-3) Cells, Antioxidants, 11, 1814, https://doi.org/10.3390/antiox11091814, 2022.

Helios Rybicka, E.: Impact of mining and metallurgical industries on the environment in Poland, Appl. Geochem., 11, 3–9, 1996.

Hofman, J., Maher, B. A., Muxworthy, A. R., Wuyts, K., Castanheiro, A., and Samson, R.: Biomagnetic Monitoring of Atmospheric Pollution: A Review of Magnetic Signatures from Biological Sensors, Environ. Sci. Technol., 51, 6648–6664, https://doi.org/10.1021/acs.est.7b00832, 2017.

Horckmans, G. P., Möckel, R., Nielsen, P., Kukurugya, F., Vanhoof, C., Morillon, A., and Algermissen D.: Multi-Analytical Characterization of Slags to Determine the Chromium Concentration for a Possible Re-Extraction, Minerals, 9, 646, https://doi.org/10.3390/min9100646, 2019.

Huffman, G. P., Huggins, F. E., and Dunmyre, G. R.: Investigation of the high-temperature behaviour of coal ash in reducing and oxidizing atmospheres, Fuel, 60, 585–597, https://doi.org/10.1016/0016-2361(81)90158-7, 1981.

Ito, A., Lin, G., and Penner, J. E.: Radiative forcing by light-absorbing aerosols of pyrogenetic iron oxides, Sci. Rep., 8, 7347, https://doi.org/10.1038/s41598-018-25756-3, 2018.

Ito, A., Myriokefalitakis, S., Kanakidou, M., Mahowald, N. M., Scanza, R. A., Hamilton, D. S., Baker, A. R., Jickells, T., Sarin, M., Bikkina, S., Gao, Y., Shelley, R. U., Buck, C. S., Landing, W. M., Bowie, A. R., Perron, M. M. G., Guieu, C., Meskhidze, N., Johnson, M. S., Feng, Y., Kok, J. F., Nenes, A., and Duc, R. A.: Pyrogenic iron: The missing link to high iron solubility in aerosols, Sci. Adv., 5, eaau7671, https://doi.org/10.1126/sciadv.aau7671, 2019.

Ito, A., Adebiyi, A. A., Huang, Y., and Kok, J. F.: Less atmospheric radiative heating by dust due to the synergy of coarser size and aspherical shape, Atmos. Chem. Phys., 21, 16869–16891, https://doi.org/10.5194/acp-21-16869-2021, 2021a.

Ito, A., Ye, Y., Baldo, C., and Shi, Z.: Ocean fertilization by pyrogenic aerosol iron, npj Clim. Atmo. Sci., 4, 30, https://doi.org/10.1038/s41612-021-00185-8, 2021b.

Jabłońska, M., Rachwał, M., Wawer, M., Kądziołka-Gaweł, M., Teper, E., Krzykawski, T., and Smołka-Danielowska, D.: Mineralogical and Chemical Specificity of Dusts Originating from Iron and Non-Ferrous Metallurgy in the

Light of Their Magnetic Susceptibility, Minerals, 11, 216, https://doi.org/10.3390/min11020216, 2021.

Jarzębski, S. and Kapała, J.: Atlas zanieczyszczeń wydzielanych przy procesach hutnictwa żelaza, Wydawnictwo Śląsk, Katowice, 345 pp., 1975.

Jenkins, N. T.: Chemistry of Airborne Particles from Metallurgical Processing, Dept. of Materials Science and Engineering, PhD Thesis, http://dspace.mit.edu/handle/1721.1/17033 (last access: 10 January 2023), 2003.

Jenkins, N. T. and Eagar, T. W.: Chemical Analysis of Welding Fume Particles, Welding Research, Suppl. Weld. J., 84, 87–93, 2005.

Li, S., Zhang, B., Wu, D., Li, Z., Chu, S.-Q., Ding, X., Tang, X., Chen, J., and Li, Q.: Magnetic Particles Unintentionally Emitted from Anthropogenic Sources: Iron and Steel Plants, Environ. Sci. Tech. Lett., 8, 295–300, https://doi.org/10.1021/acs.estlett.1c00164, 2021.

Li, W., Shao, L., Zhang, D., Ro, C.-U., Hu, M., Bi, X., Geng, H., Matsuki, A., Niu, H., and Chen, J.: A review of single aerosol particle studies in the atmosphere of East Asia: morphology, mixing state, source, and heterogeneous reactions, J. Clean. Prod., 112, 1330–1349, https://doi.org/10.1016/j.jclepro.2015.04.050, 2016.

Liati, A., Pandurangi, S. S., Boulouchos, K., Schreiber, D., and Arroyo Rojas Dasilva, Y.: Metal nanoparticles in diesel exhaust derived by in-cylinder melting of detached engine fragments, Atmos. Environ., 101, 34–40, https://doi.org/10.1016/j.atmosenv.2014.11.014, 2015.

Liu, H., Yan, Y., Chang, H., Chen, H., Liang, L., Liu, X., Qiang, X., and Sun, Y.: Magnetic signatures of natural and anthropogenic sources of urban dust aerosol, Atmos. Chem. Phys., 19, 731–745, https://doi.org/10.5194/acp-19-731-2019, 2019.

Liu, L., Li, L., Lin, Q., Wang, Y., Zhang, J., Zhu, Z., Yuan, Q., Zhou, S., Zhang D., Baldo, C., and Shi, Z.: Size-dependent aerosol iron solubility in an urban atmosphere, npj Clim. Atmos. Sci., 5, 53, https://doi.org/10.1038/s41612-022-00277-z, 2022.

Lodovici, M. and Bigagli, E.: Oxidative Stress and Air Pollution Exposure, J. Toxicol., 2011, 487074, https://doi.org/10.1155/2011/487074, 2011.

Lu, D., Luo, Q., Chen, R., Zhuansun, Y., Jiang, J., Wang, W., Yang, X., Zhang, L., Liu, X., Li, F., Liu, Q., and Jiang, G.: Chemical multi-fingerprinting of exogenous ultrafine particles in human serum and pleural effusion, Nat. Commun., 11, 2567, https://doi.org/10.1038/s41467-020-16427-x, 2020.

Mackey, K. R. M., Chien, C.-T., Post, A. F., Saito, M. A., and Paytan, A.: Rapid and gradual modes of aerosol trace metal dissolution in seawater, Front. Microbiol., 5, 794, https://doi.org/10.3389/fmicb.2014.00794, 2015.

Magiera, T., Strzyszcz, Z., Jabłońska, M., and Bzowska, G.: Characterization of magnetic particulates in urban and industrial dusts, WIT Trans. Ecol. Envir., 136, 171–184, https://doi.org/10.2495/AIR100161, 2010.

Magiera, T., Górka-Kostrubiec, B., Szumiata, T., and Wawer, M.: Technogenic magnetic particles from steel metallurgy and iron mining in topsoil: Indicative characteristic by magnetic parameters and Mössbauer spectra, Sci. Total Environ., 775, 145605, https://doi.org/10.1016/j.scitotenv.2021.145605, 2021.

Maher, B. A.: Rain and Dust: Magnetic Records of Climate and Pollution, Elements, 5, 361–375, https://doi.org/10.2113/gselements.5.4.229, 2009.

Maher, B. A.: Airborne Magnetite- and Iron-Rich Pollution Nanoparticles: Potential Neurotoxicants and Environmental Risk Factors for Neurodegenerative Disease, Including Alzheimer's Disease, J. Alzheimer's Dis., 71, 229–234, https://doi.org/10.3233/JAD-190204, 2019.

Maher, B. A., Ahmed, I. A. M., Karloukovski, V., MacLaren, D. A., Foulds, P. G., Allsop, D., Mann, D. M. A., Torres-Jardón, R., and Calderon-Garciduenas, L.: Magnetite pollution nanoparticles in the human brain, P. Natl. Acad. Sci. USA, 113, 10797–10801, https://doi.org/10.1073/pnas.1605941113, 2016.

Maher, B. A., González-Maciel, A., Reynoso-Robles, R., Torres-Jardón, R., and Calderón-Garcidueñas, L.: Iron-rich air pollution nanoparticles: An unrecognised environmental risk factor for myocardial mitochondrial dysfunction and cardiac oxidative stress, Environ. Res., 188, 109816, https://doi.org/10.1016/j.envres.2020.109816, 2020.

Mahowald, N. M., Hamilton, D. S., Mackey, K. R. M., Moore, J. K., Baker, A. R., Scanza, R. A., and Zhang, Y.: Aerosol trace metal leaching and impacts on marine microorganisms, Nat. Commun., 9, 2614, https://doi.org/10.1038/s41467-018-04970-7, 2018.

Manke, A., Wang, L., and Rojanasakul, Y.: Mechanisms of Nanoparticle-Induced Oxidative Stress and Toxicity, Biomed Res. Int., 2013, 942916, https://doi.org/10.1155/2013/942916, 2013.

Mejía-Echeverry, D., Chaparro, M. A. E., Duque-Trujillo, J. F., Chaparro, M. A. E., and Castañeda Miranda, A. G: Magnetic Biomonitoring as a Tool for Assessment of Air Pollution Patterns in a Tropical Valley Using Tillandsia sp, Atmosphere-Basel, 9, 283, https://doi.org/10.3390/atmos9070283, 2018.

Moreno, T., Martins, V., Querol, X., Jones, T., BéruBé, K., Minguillón, M. C., Amato, F., Capdevila, M., de Miguel, E., Centelles, S., and Gibbons, W.: A new look at inhalable metalliferous airborne particles on rail subway platforms, Sci. Total Environ., 505, 367–375, https://doi.org/10.1016/j.scitotenv.2014.10.013, 2015.

Morris, W. A., Versteeg, J. K., Bryant, D. W., Legzdins, A. E., McCarry, B. E., and Marvin, C. H.: Preliminary comparisons between mutagenicity and magnetic susceptibility of respirable airborne particulate, Atmos. Environ., 29, 3441–3450, https://doi.org/10.1016/1352-2310(95)00203-B, 1995.

Moteki, N., Adachi, K., Ohata, S., Yoshida, A., Harigaya, T., Koike, M., and Kondo, Y.: Anthropogenic iron oxide aerosols enhance atmospheric heating, Nat. Commun., 8, 15329, https://doi.org/10.1038/ncomms15329, 2017.

Murad, E. and Cashion, J.: Mössbauer Spectroscopy of Environmental Materials and Their Industrial Utilization, Springer US, Boston, MA, https://doi.org/10.1007/978-1-4419-9040-2, 2004.

Muxworthy, A. R., Matzka, J., Davila, A. F., and Petersen, N.: Magnetic signature of daily sampled urban atmospheric particles, Atmos. Environ., 37, 4163–4169, https://doi.org/10.1016/S1352-2310(03)00500-4, 2003.

Neuhold, S., van Zomeren, A., Dijkstra, J. J., van der Sloot, H. A., Drissen, P., Algermissen, D., Mudersbach, D., Schüler, S., Griessacher, T., Raith, J. G., Pomberger, R., and Vollprecht, D.: Investigation of Possible Leaching Control Mechanisms for Chromium and Vanadium in Electric Arc Furnace (EAF) Slags

Using Combined Experimental and Modeling Approaches, Minerals, 9, 525, https://doi.org/10.3390/min9090525, 2019.

Paytan, A., Mackey, K. R. M., Chen, Y., Lima, I. D., Doney, S. C., Mahowald, N., Labiosa, R., and Post, A. F.: Toxicity of atmospheric aerosols on marine phytoplankton, P. Natl. Acad. Sci. USA, 106, 4601–4605, https://doi.org/10.1073/pnas.0811486106, 2009.

Petrovský, E., Zbořil, R., Grygar, T. M., Kotlík, B., Novák, J., Kapička, A., and Grison, H.: Magnetic particles in atmospheric particulate matter collected at sites with different level of air pollution, Stud. Geophys. Geod., 57, 755–770, https://doi.org/10.1007/s11200-013-0814-x, 2013.

Pietrodangelo, A., Pareti, S., and Perrino, C.: Improved identification of transition metals in airborne aerosols by SEM–EDX combined backscattered and secondary electron microanalysis, Environ. Sci. Pollut. Res., 21, 4023–4031, https://doi.org/10.1007/s11356-013-2261-1, 2014.

Potysz, A. and Kierczak, J.: Prospective (Bio)leaching of Historical Copper Slags as an Alternative to Their Disposal, Minerals, 9, 542, https://doi.org/10.3390/min9090542, 2019.

Revuelta, M. A., McIntosh, G., Pey, J., Pérez, N., Querol, X., and Alastuey, A.: Partitioning of magnetic particles in PM_{10}, $PM_{2.5}$ and PM_1 aerosols in the urban atmosphere of Barcelona (Spain), Environ. Pollut., 188, 109–117, https://doi.org/10.1016/j.envpol.2014.01.025, 2014.

Řezníček, R., Chlan, V., Štěpánková, H., Novák, P., Żukrowski, J., Kozłowski, A., Kąkol, Z., Tarnawski, Z., and Honig, J. M.: Understanding the Mössbauer spectrum of magnetite below the Verwey transition: *Ab initio* calculations, simulation, and experiment, Phys. Rev. B, 96, 195124, https://doi.org/10.1103/PhysRevB.96.195124, 2017.

Rodríguez-Carvajal, J.: Recent advances in magnetic structure determination by neutron powder diffraction, Phys. Condens. Matter, 192, 55–69, https://doi.org/10.1016/0921-4526(93)90108-I, 1993.

Rutkowski, R., Bihałowicz, J. S., Rachwał, M., Rogula-Kozłowska, W., and Rybak, J.: Magnetic Susceptibility of Spider Webs and Dust: Preliminary Study in Wrocław, Poland, Minerals, 10, 118, https://doi.org/10.3390/min10111018, 2020.

Sagnotti, L., Macrì, P., Egli, R., and Mondino, M.: Magnetic properties of atmospheric particulate matter from automatic air sampler stations in Latium (Italy): Toward a definition of magnetic fingerprints for natural and anthropogenic PM_{10} sources, J. Geophys. Res.-Sol. Ea., 111, B12S22, https://doi.org/10.1029/2006JB004508, 2006.

Sorensen, M.: Transition Metals in Personal Samples of $PM_{2.5}$ and Oxidative Stress in Human Volunteers, Cancer Epidem. Biomar., 14, 1340–1343, https://doi.org/10.1158/1055-9965.EPI-04-0899, 2005.

Shahpoury, P., Zhang, Z. W., Arangio, A., Celo, V., Dabek-Zlotorzynska, E., Harner, T., and Nenes, A.: The influence of chemical composition, aerosol acidity, and metal dissolution on the oxidative potential of fine particulate matter and redox potential of the lung lining fluid, Environ. Int., 148, 106343, https://doi.org/10.1016/j.envint.2020.106343, 2021.

Spassov, S., Egli, R., Heller, F., Nourgaliev, D. K., and Hannam, J.: Magnetic quantification of urban pollution sources in atmospheric particulate matter, Geophys. J. Int., 159, 555–564, https://doi.org/10.1111/j.1365-246X.2004.02438.x, 2004.

Tong, Y., Li, A., Cai, Y., Ni, X., Zhang, Y., Wang, J., Guo, P., Li, X., and Zhang: Mössbauer Study of Atmospheric Aerosols of Shanghai, Environ. Sci. Technol., 35, 1432–1436, https://doi.org/10.1021/es0016497, 2001.

Wang, J., Li, S., Li, H., Qian, X., Li, X., Liu, X., Lu, H., Wang, C., and Sun, Y.: Trace metals and magnetic particles in $PM_{2.5}$: Magnetic identification and its implications, Sci. Rep., 7, 9865, https://doi.org/10.1038/s41598-017-08628-0, 2017.

Wilczyńska-Michalik, W.: Mineralogical study of dusts emitted by Lenin's Steel Plant in Kraków, Polska Akademia Nauk – Oddziałw Krakowie, Komisja Nauk Mineralogicznych, Prace Mineralogiczne 68, 5–52, 1981 (in Polish with English summary).

Wilczyńska-Michalik, W., Dańko, J., and Michalik, M.: Characteristics of particulate matter emitted from a coal-fired power plant, Pol. J. Env. Stud., 29, 1411–1420, https://doi.org/10.15244/pjoes/106034, 2020a.

Wilczyńska-Michalik, W., Michalik, J. M., Kapusta, C., and Michalik, M.: Airborne Magnetic Technoparticles in Soils as a Record of Anthropocene, Atmosphere-Basel, 11, 44, https://doi.org/10.3390/atmos11010044, 2020b.

Wirth, E. and Prodi, F.: The concentration and size distribution of airborne ferromagnetic particles, Tellus, 24, 561–567, https://doi.org/10.3402/tellusa.v24i6.10683, 1972.

Yamada, Y. and Nishida, N.: Iron-based Nanoparticles and Their Mössbauer Spectra, Radioisotopes, 68, 125–143, https://doi.org/10.3769/radioisotopes.68.125, 2019.

Zhang, Q., Lu, D., Wang, D., Yang, X., Zuo, P., Yang, H., Fu, Q., Liu, Q., and Jiang, G.: Separation and Tracing of Anthropogenic Magnetite Nanoparticles in the Urban Atmosphere, Environ. Sci. Technol., 54, 9274–9284, https://doi.org/10.1021/acs.est.0c01841, 2020.